DOI: 10.1002/chem.201000841

Luminescent Quantum Clusters of Gold in Bulk by Albumin-Induced Core Etching of Nanoparticles: Metal Ion Sensing, Metal-Enhanced Luminescence, and Biolabeling

Madathumpady Abubaker Habeeb Muhammed,[a] Pramod Kumar Verma,[b] Samir Kumar Pal,[b] Archana Retnakumari,[c] Manzoor Koyakutty,[c] Shantikumar Nair,[c] and Thalappil Pradeep*[a]

Dedicated to Professor R. Graham Cooks

Abstract: The synthesis of a luminescent quantum cluster (QC) of gold with a quantum yield of ~4% is reported. It was synthesized in gram quantities by the core etching of mercaptosuccinic acid protected gold nanoparticles by bovine serum albumin (BSA), abbreviated as Au_{QC}@BSA. The cluster was characterized and a core of Au_{38} was assigned tentatively from mass spectrometric analysis. Luminescence of the QC is exploited as a "turn-off" sensor for Cu^{2+} ions and a "turn-on" sensor for glutathione detection. Metal-enhanced luminescence (MEL) of this QC in the presence of silver nanoparticles is demonstrated and a ninefold maximum enhancement is seen. This is the first report of the observation of MEL from QCs. Folic acid conjugated Au_{QC}@BSA was found to be internalized to a significant extent by oral carcinoma KB cells through folic acid mediated endocytosis. The inherent luminescence of the internalized Au_{QC}@BSA was used in cell imaging.

Keywords: core etching · luminescence · nanoparticles · quantum clusters · sensors

Introduction

Among the various nanostructures synthesized in the recent past, quantum clusters (QCs) or sub-nanoclusters are attracting enormous attention due to their novel optical and electronic properties. They are composed of very few atoms, with a core size in the sub-nanometer regime, which is the reason for the name sub-nanocluster.[1–35] Owing to the sub-nanometer core size, they cannot possess continuous density of states but have discrete electronic energy levels. Consequently they show "molecule-like" optical transitions in absorption and emission and can be termed also as molecular clusters. Because these QCs behave entirely differently from the metallic nanoparticles of the same element, their scope in different areas of science and technology is very large. One of the most promising properties of QCs is their photoluminescence with decent quantum yield (QY).[3–10] QCs with a QY as high as 70% have been reported.[4,5] It is also possible to tune their emission wavelength from the ultraviolet (UV) to the near-infrared (NIR) range by changing the number of core atoms. Dickson et al. reported the synthesis of dendrimer-encapsulated gold QCs with cores ranging from Au_5 to Au_{31}, and with luminescence ranging from blue to the NIR region.[4,5] There have been several detailed investigations of the photoluminescence of QCs. Because QCs are highly luminescent and biocompatible due to their lower metallic content, they hold great promise as ultrabright, biocompatible biolabels and light-emitting sources in

[a] M. A. Habeeb Muhammed, Prof. T. Pradeep
DST Unit on Nanoscience (DST UNS)
Department of Chemistry and
Sophisticated Analytical Instrument Facility
Indian Institute of Technology Madras
Chennai 600 036 (India)
Fax: (+91) 44-2257-0509
E-mail: pradeep@iitm.ac.in

[b] P. K. Verma, Prof. S. K. Pal
Unit for Nanoscience and Technology
Department of Chemical, Biological and Macromolecular Sciences
Satyendra Nath Bose National Centre for Basic Sciences
Block JD, Sector III, Salt Lake, Kolkata 700 098 (India)

[c] A. Retnakumari, Prof. M. Koyakutty, Prof. S. Nair
Amrita Centre for Nanoscience and Molecular Medicine
Amrita Institute of Medical Science
Cochin 682 041 (India)

Supporting information for this article is available on the WWW under http://dx.doi.org/10.1002/chem.201000841.

the nanoscale, and hence can be used in imaging, detection, and so on.[6–8] Unlike organic dyes, they are photostable,[6] a quality that widens their potential applications. These QCs can be readily conjugated with several biological molecules, which further enhance their application potential. A recent report based on cell viability and reactive oxygen toxicity studies showed that the gold QCs are nontoxic up to relatively high concentrations of 500 $\mu g\,mL^{-1}$.[7] Two-photon emission, a process in which transition between energy levels occurs through the simultaneous emission of two photons, is observed in Au_{25} QCs and hence they can be made useful for two-photon imaging with IR excitation.[9] Förster resonance energy transfer (FRET) between the metal core and the ligand in $Au_{25}SG_{18}$ (SG: glutathione thiolate) has been demonstrated by using dansyl chromophores attached to the QC core through glutathione linkers.[10] Photon antibunching, a quantum phenomenon that occurs during luminescence, in which the emission of one photon reduces the probability that another photon will be emitted immediately afterwards, was observed in Au_{23} QCs synthesized inside the dendrimer cavities.[5] QCs also exhibit electroluminescence at room temperature and hence provide facile routes to produce strong single-photon emitters.[17,18]

There are several methods reported for the synthesis of both water-soluble[3–23] and organic-soluble[24–33] QCs of gold. All the various methods developed so far for the synthesis of QCs can be broadly classified into four categories. The first method is the direct synthesis of QCs by the reduction of gold ions in the presence of suitably selected ligands or templates. A series of glutathione-capped gold QCs has been synthesized by reducing gold ions in the presence of glutathione, followed by their separation using polyacrylamide gel electrophoresis (PAGE).[12] Several organic-soluble QCs, such as Au_{25},[26] Au_{20},[27] and Au_{38},[28] have been synthesized by this method. The second method involves the usage of biomolecules such as dendrimers[3–5] and proteins[20] as scaffolds for the synthesis of QCs. The third method is the conversion of an already existing QC into another one. Tsukuda et al. showed that among the various glutathione-protected QCs, Au_{25} is the most thermodynamically stable and larger analogues can be converted to Au_{25} by adding excess glutathione.[14] The same group also synthesized Au_{25} QCs from phosphine-capped Au_{11} QCs in the presence of glutathione.[15] We have recently reported the synthesis of Au_{22}, Au_{23}, and Au_{33} QCs from Au_{25} by following single-phase and interfacial techniques.[8] The last method is the synthesis of QCs by the core etching of metallic nanoparticles of the same element. In this method, a nanoparticle is treated with excess amounts of molecules such as thiols,[19,29] dendrimers,[34] and Au^{3+}[6] ions, which can etch the core of the metallic nanoparticle leading to the formation of QCs. Duan and Nie synthesized a blue-emitting Au_8 QC by the core etching of dodecylamine-capped gold nanoparticles (AuNPs) by polyethylenimine (PEI).[34] Two different QCs with Au_{25} and Au_8 cores have been synthesized from mercaptosuccinic acid (MSA) capped AuNPs by etching with glutathione at two different pH values.[19] A red-emitting gold QC was synthesized recently by etching organic-soluble didodecyldimethylammonium bromide capped AuNPs with gold ions and subsequently transferring it to the aqueous phase by dihydrolipoic acid.[6] A facile conversion of polydisperse AuNPs into well-defined monodisperse 25-atom nanorods and nanospheres has been reported.[29]

Herein, we report the synthesis of a luminescent QC of gold with a QY of ~4% starting from AuNPs, by employing the core etching method. We and several other groups have employed the method of core etching to synthesize QCs from nanoparticles.[6,19,29] However, the QY of the QCs produced was not appreciable for its application in diverse fields. Apart from the conventional chemicals that are widely used for reduction and stabilization of nanoparticles, biomolecules are also known for their role in nanoparticle synthesis for reduction and/or stabilization.[36–40] Several molecules, such as dendrimers,[3–5] proteins,[20] and DNA,[35] act as templates for QC synthesis. Even though the complete synthetic mechanism is unknown, the use of these biomolecules is a step towards developing green chemistry protocols for QC synthesis. Here, we use bovine serum albumin (BSA) as the etching agent. BSA has long been used as a capping agent for preformed nanoparticles. Recently, Ying et al.[20] synthesized highly luminescent gold QCs using the reduction capacity of BSA at pH 12. BSA is a large globular protein (66000 Da) with 583 amino acid residues. It is also known as "Fraction V" and is a serum albumin protein that has numerous biochemical applications. BSA is used widely in scientific research because of its stability, its lack of effect in many biochemical reactions, and its low cost. The QC synthesized is characterized thoroughly and the luminescence of the QC is exploited as a "turn-off" sensor for the detection of the Cu^{2+} ion and a "turn-on" sensor for glutathione detection. We also showed metal-enhanced luminescence (MEL) of this QC in the presence of silver nanoparticles (AgNPs). This is the first report of the observation of MEL from QCs. We also exploited the inherent luminescence of this cluster for the imaging of oral carcinoma KB cells by folic acid (FA) mediated endocytosis.

Results and Discussion

MSA-capped AuNPs (Au_{NP}@MSA) are taken as the precursor for the synthesis of QCs. The nanoparticles were synthesized by the reduction of gold ions in the presence of MSA. This method produced small nanoparticles of core diameter 2–3 nm. The nanoparticle showed an almost featureless exponential-type optical absorption spectrum (Supporting Information, Figure S1). It is known that AuNPs with core diameter $\leq$2 nm will not possess surface plasmon resonance.[45] For the QC synthesis, Au_{NP}@MSA in water was mixed with BSA, 1:10 by weight, in air under constant stirring. The pH of the solution was adjusted to 12 after 5 min and stirring was continued at 37 °C. Formation of QCs was monitored by checking the luminescence spectra of the solution at regular intervals of time. The starting material,

Au_{NP}@MSA, showed negligible luminescence. As the reaction progressed, a gradual increase in the luminescence from the solution was observed. This increase of luminescence was also monitored visually by irradiating the solution with a UV lamp of 350 nm excitation wavelength at various stages of reaction. After around 6–8 h of reaction, there was no further enhancement in the luminescence and the reaction was terminated. The color of the solution changed from dark brown to reddish brown. The solution was centrifuged to remove the unreacted nanoparticles. The QCs were further purified by dialysis for 24 h with a water change after every 8 h. The solution obtained after dialysis was subjected to freeze-drying to obtain QCs in the powder form, which was redispersed in water for further characterization. The QC synthesized by this route is termed Au_{QC}@BSA from now on.

The UV/Vis absorption spectrum of Au_{QC}@BSA is shown in Figure 1. The spectrum is almost featureless but has a different slope around 375 nm. The optical absorption spectrum showed a gradual rise at 800 nm with a continuous increase in absorbance afterwards. The spectrum was different from that of the parent Au_{NP}@MSA. Prior studies showed

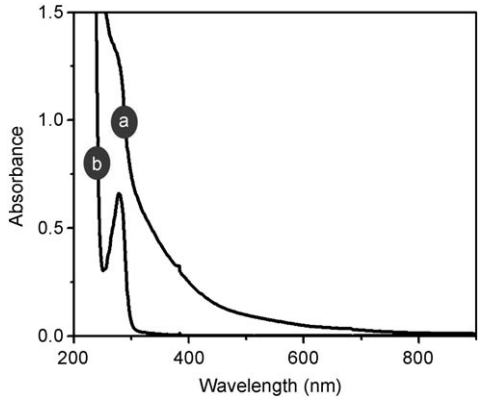

Figure 1. Optical absorption spectrum of Au_{QC}@BSA (trace a) compared with that of free BSA (trace b). The absorbance shows a gradual rise at 800 nm.

that QCs of gold can be classified into two groups based on their optical properties.[12] The first group are called "thiolated" QCs. They show well-defined characteristic absorption features due to intraband (sp to sp) and interband (sp to d) transitions.[30] Thiolated QCs are generally protected with water- or organic-soluble thiols. Their QY is comparatively low. On the other hand, the second group of QCs are known as "free-falling" QCs and do not show well-defined characteristic absorption features, unlike the thiolated QCs, and their QY is comparatively high. They are encapsulated by biomolecules such as dendrimers or proteins. So it can be said that ligands play a crucial role in determining the photophysical properties of gold QCs. The QC produced here is presumed to be encapsulated by BSA (as confirmed by the mass spectrum), and therefore well-defined absorption features are not observed in the optical absorption spectrum, following the general trend. It is known that ligands such as thiols[29] and dendrimers[34] can perform core etching of nanoparticles with ligand exchange. When they are added in limited quantity, only ligand exchange happens. However, when they are added in excess, core etching with complete ligand exchange occurs. For example, when MSA-protected nanoparticles are etched with glutathione, the MSA protection is completely removed.[19] Therefore, in the present case we also expect that the MSA molecules are removed completely, even though we do not have solid evidence for their complete absence. The mechanism of cluster formation is unclear at this moment. There are two possibilities. The first is that BSA can etch the surface atoms of nanoparticles, thus leading to core-size reduction and producing clusters. The second is that gold atoms removed from nanoparticles by core etching may undergo aurophilic interactions to form the cluster, as there is a tendency for gold(I) compounds to form oligomers, chains, or layers by means of gold(I)–gold(I) interactions due to hybridization of the empty 6s/6p and filled 5d orbitals. The second possibility is less likely in view of the dominant Au^0 characteristic of the cluster in X-ray photoelectron spectroscopy (XPS).

Figure 2 compares the photoluminescence profiles of pure BSA (traces i and ii) with those of Au_{QC}@BSA (traces iii and iv). Although excitation of Au_{QC}@BSA had two peaks, one at 370 nm and the other at 510 nm, the emission maximum was 660 nm. Pure BSA shows excitation and emission at 290 and 345 nm, respectively. The QC showed observable red emission when the aqueous solution was irradiated by a UV lamp at room temperature (Figure 2B). It also showed luminescence in the solid powder form (Figure 2E). The lu-

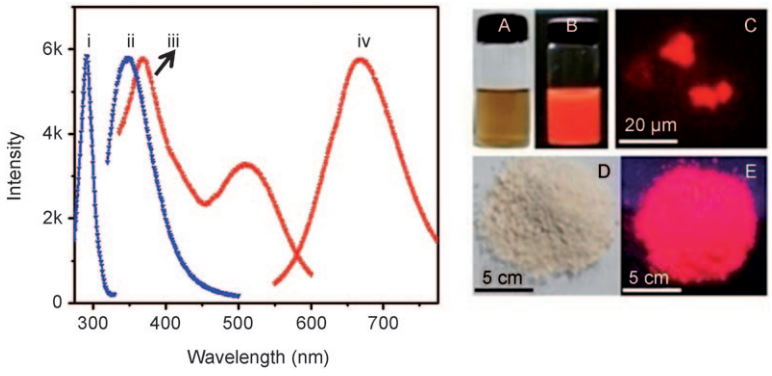

Figure 2. Left: Photoluminescence profiles of BSA (traces i and ii) and Au_{QC}@BSA (traces iii and iv). Right: photographs of Au_{QC}@BSA solution under white light (A) and UV light (B), confocal luminescence image of the QC (C), and photographs of QC powder under irradiation by white light (D) and UV light (E).

minescence from solid Au_{QC}@BSA was imaged by confocal fluorescence microscopy (Figure 2C). Au_{QC}@BSA dissolved in ultrapure water was drop-cast on a glass slide, dried, covered with a coverslip, and illuminated at 405 nm. A strong luminescence was seen from the various islands formed by Au_{QC}@BSA. QCs were imaged at different wavelengths from 540 to 630 nm (maximum range possible in the instrument) and showed maximum luminescence at a wavelength of 630 nm (Supporting Information, Figure S2). The luminescence from the QCs may be due to the interband transitions between the filled $5d^{10}$ band and $6(sp)^1$ conduction band.[12] The QY of the QC is ~4%. The luminescence decay of the QC in water was measured by a picosecond-resolved time-correlated single-photon counting (TCSPC) technique (Supporting Information, Figure S3). The numerical fitting of the luminescence collected at 660 nm revealed time constants of 0.10 (59.6%), 0.86 (21.9%), 4.5 (8.6%), and 174.7 ns (9.9%).

Unlike metallic nanoparticles, which are addressed in terms of their core diameter, QCs are represented in terms of their chemical composition. To find the number of gold atoms in the core of the QC, mass spectrometric analysis was carried out by matrix-assisted laser desorption/ionization (MALDI) mass spectrometry (MS). On the other hand, electrospray ionization mass spectrometry (ESIMS) in the orthogonal geometry, as in our QTrap 3200 instrument, does not give features due to intact QCs as reported previously.[12] Sinapinic acid was used as the matrix for MALDI. Tetrafluoroacetic acid (TFA) was added to enhance the ionization. In the absence of TFA, no peaks were observed. The spectrum was collected in the negative mode and averaged for 100 shots. MALDI-MS of pure BSA showed a singly charged peak at m/z 66.7 kDa (Figure 3). On the other hand, for Au_{QC}@BSA a peak at reduced intensity was observed at ~74.1 kDa in addition to the peak at 66.7 kDa, which is assigned to the QC–BSA complex. The difference between the QC–BSA complex and BSA corresponds to 38 gold atoms and hence we can tentatively assign a core of Au_{38} to the QC formed here. A precise estimation of the nuclearity needs better mass spectral data. As we did not observe any peak with m/z higher than 74.1 kDa, we assume that all the clusters have this core. Detailed studies on mass spectra are required to establish the correct chemical composition, particularly in view of the reduced intensity. Comparing the mass spectra of BSA and Au_{QC}@BSA, certain important differences may be noted. The spectral intensity is reduced in the case of QCs with a substantial broadening of the features. These changes can be attributed to the modification of the protein structure during QC synthesis, which retarded ion formation.

To assign the core size, Au_{QC}@BSA was analyzed by high-resolution transmission electron microscopy (HRTEM). QCs with an average size of 1 nm are seen in the TEM image (Figure 4A) and no particles of larger size were observed. The QCs were very sensitive towards the electron beam and they aggregated to form bigger nanoparticles upon longer electron-beam irradiation of the sample, due to core fusion as is typical of QCs in this size range.[46] Figure 4B shows the 4f core-level photoemission spectrum of Au_{QC}@BSA. Binding energies (BEs) of the cluster were 84.5 eV for $4f_{7/2}$ and 88.2 eV for $4f_{5/2}$. Tsukuda et al. reported that the BE of $4f_{7/2}$ of the gold QCs comes in between 84 and 86 eV, that is, between the BE values of gold film and gold thiolate.[12]

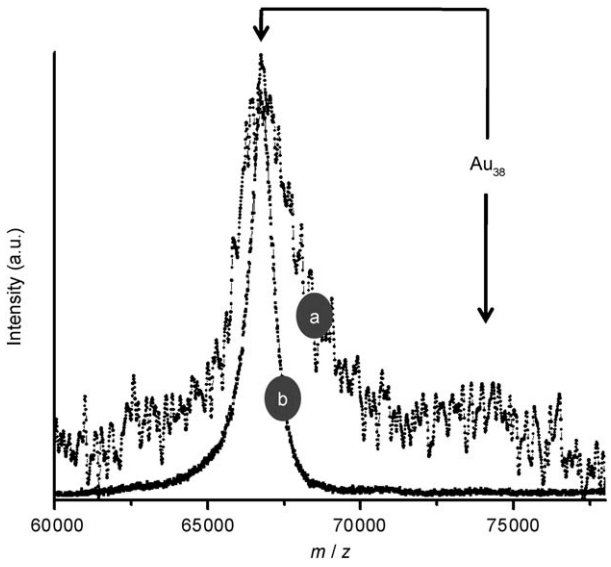

Figure 3. MALDI-MS of Au_{QC}@BSA (trace a) and BSA (trace b). The spectrum of Au_{QC}@BSA is weaker and has been enlarged to show the features.

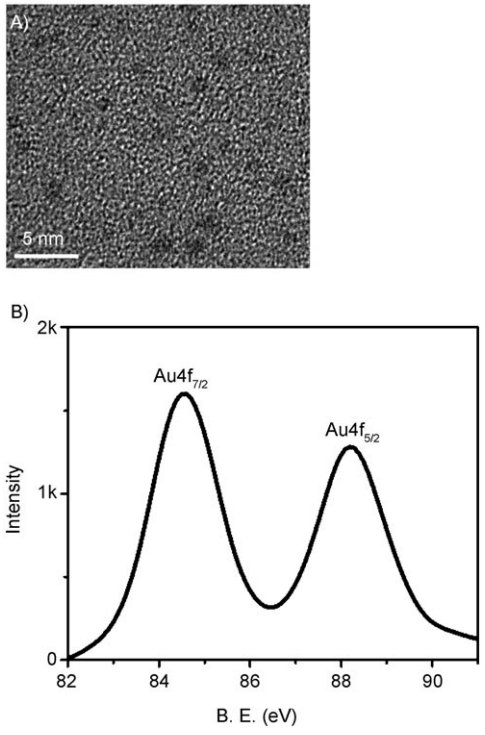

Figure 4. A) HRTEM image and B) Au (4f) XPS spectrum of Au_{QC}@BSA. The gold core is visible in the TEM image on closer examination.

To check the presence of gold and other elements, energy-dispersive X-ray (EDX) analysis was carried out (Supporting Information, Figure S4) by drop-casting an aqueous solution of the QC on indium tin oxide (ITO) glass plates. The elements present in the QCs were mapped and the images are presented in the Supporting Information, Figure S4.

The nature of ligand protection of the QCs can be studied by using their FTIR spectra, which give features resulting from the ligands. The FTIR spectrum of the QC is compared with that of pure BSA in the Supporting Information, Figure S5A. The black trace depicts the spectrum of pure BSA and the red trace is the spectrum of Au_{QC}@BSA. Our interest here is to check what structural changes the capping BSA molecules undergo on the QC surface. The bending and stretching vibrations that characterize the secondary structure of the peptide backbone were monitored. There are two regions (1700–1600 and 1550–1500 cm^{-1}) in the spectrum, unique to the protein secondary structure, called amide I and amide II.[47,48] In pure BSA, the amide I and amide II vibrations were found to occur at 1655 and 1539 cm^{-1} (black trace, Figure S5B), respectively. Their position in Au_{QC}@BSA does not undergo any change (red trace, Figure S5B). To check whether any conformational changes occur in BSA, circular dichroism (CD) spectroscopy was performed. CD is very useful to study three-dimensional structures of proteins. Each of the three basic secondary structures of a polypeptide chain (helix, sheet, and coil) shows a characteristic CD spectrum, and from it we can derive the percentage of α-helical, β-sheet, or random-coil structures.[40,41] For the α-helical structure of protein, two negative minima at 208 and 222 nm are present in pure BSA (black trace, Figure S5C). For the Au_{QC}@BSA, these peaks were observed at 206 and 219 nm (red trace, Figure S5C). This indicates that a slight conformational change has happened when BSA is on the QC surface. The percentage of various conformations has been determined for both pure BSA and Au_{QC}@BSA (Supporting Information, Table S1). From the analysis, it can be inferred that the percentage of α-helical structure is changed upon QC formation. The surface electrical properties of proteins have an important influence on the performance of most of the separation processes. The surface charge of proteins arises from ionization of the acidic and basic side chains of the amino acids constituting the protein. These ionization reactions are acid–base equilibria and thus depend on the pH of the solution. The zeta potentials of BSA and Au_{QC}@BSA were measured at pH 3, 7, and 12 (Supporting Information, Figure S5D). BSA is reported to have an isoelectric point at pH 4.7. So BSA will be positively charged below pH 4.7 and negatively charged above pH 4.7. Zeta potential measurements of both BSA and Au_{QC}@BSA showed similar values at various pH levels. This finding indicates that no modification of the surface electric property of BSA has occurred due to QC formation. This is important for biological applications.

The luminescence of the as-prepared QC can be used as a highly sensitive and selective luminescence "turn-off" sensor for the Cu^{2+} ion. No further modification of the QC was required for this application. Here, the effect of the luminescence of the QC in the presence of various metal ions was studied. The ions selected were Au^{3+}, Ag^{+}, Cu^{2+}, Ni^{2+}, Ca^{2+}, Mg^{2+}, Na^{+}, Pb^{2+}, Hg^{2+}, Zn^{2+}, Sm^{2+}, Fe^{3+}, Co^{2+}, and Cd^{2+} as their nitrates or chlorides. Metal ions were added to aqueous solutions of the QC (1 mg mL^{-1}) such that the final concentration was 1 μM and the emission of the QC was measured immediately after the addition of ions. Even though there was a slight quenching of luminescence in the presence of Co^{2+}, the emission was quenched almost completely only in the presence of Cu^{2+} and remained unaltered in the presence of the other metal ions. Figure 5A is the plot of QC emission intensity against the metal ions added. Photographs of the aqueous solutions of QCs under irradiation by UV light after the addition of various metal ions are also given (Figure 5B). The specific reactivity towards Cu^{2+} can be used as a tool to detect its presence. The emission of the QC quenched as a function of Cu^{2+} concentration is shown in Figure 5C. The minimum concentration of Cu^{2+} that could be detected was 15 nM and the emission intensity decreased systematically with the increase in Cu^{2+} ion concentration.

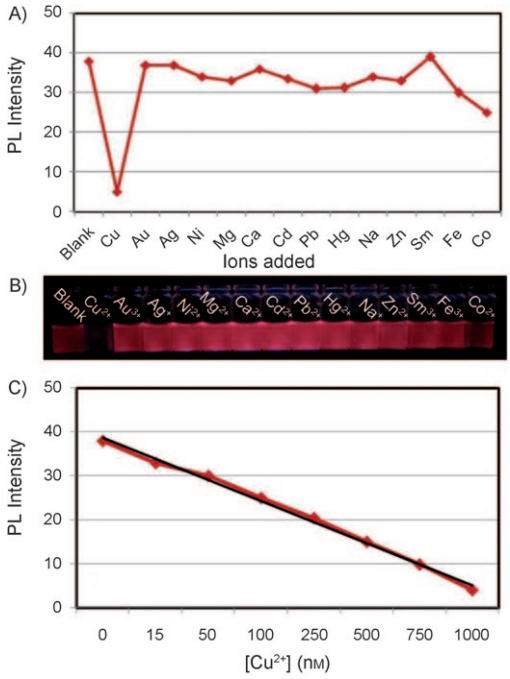

Figure 5. A) Plot of photoluminescence (PL) intensity of Au_{QC}@BSA in the presence of various metal ions. B) Photographs of aqueous solutions of the QC in the presence of the corresponding ions under irradiation by UV light. C) Plot of PL intensity of the QC as a function of $[Cu^{2+}]$ ($y = -4.803x + 43.51$ and $R^2 = 0.995$).

The luminescence quenching in the presence of Cu^{2+} can be attributed to the QC aggregation induced by the complexation between BSA and the Cu^{2+} ion. Human serum albumin (HSA) and BSA contain a high-affinity site for Cu^{II}; the binding involves both histidyl and carboxyl groups.[49]

The quenching of luminescence occurs due to the interaction between the BSA shell of the cluster and Cu^{2+} ions. There is no direct reaction between the cluster and ions. When Cu^{2+} ions are added to the aqueous solution of QCs, they mediate the protein–protein interaction and lead to spherical aggregation of Au_{QC}@BSA. When the clusters are aggregated in the presence of copper ions, the luminescence of the cluster quenches. This effect is called aggregation-induced luminescence quenching. The Cu^{2+} ion has more affinity towards BSA than any other ions. The binding constant for the copper ion is 3.6×10^9, which is high compared with that of other ions.[59] To check whether any aggregation occurred during the interaction with Cu^{2+}, the sample was analyzed by HRTEM. TEM images of the sample obtained are shown in Figure 6. Scanning of the sample at low magnification (Figure 6A) shows several spheres of varying sizes. The formation of spheres may be due to the aggregation of QCs by Cu^{2+} ions. The size of the spheres is much higher than that of the individual QCs before treatment with the Cu^{2+} ions. This confirms that the Cu^{2+} ion induced aggregation of the QCs. To see individual QCs, a spherical aggregate was selected and examined thoroughly at higher magnification (Figure 6B). Very faint dots of QCs are seen immediately after electron-beam exposure. Because the QC is nonmetallic in nature and prone to electron-beam-induced coalescence,[46] nanoparticles started to be formed during electron-beam irradiation for longer periods (Supporting Information, Figure S6). Formation of spherical aggregates was also proven by SEM. The EDX analysis of the aggregate (Supporting Information, Figure S7) shows the presence of Cu uniformly throughout the sphere, in addition to gold.

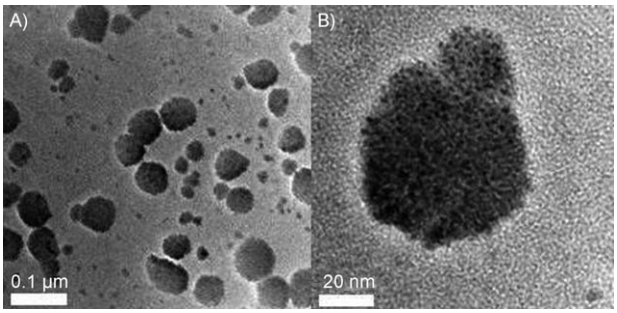

Figure 6. Lower magnification (A) and higher magnification (B) TEM images showing the aggregation of Au_{QC}@BSA upon the addition of Cu^{2+} ions.

To confirm whether the complex formation between BSA and Cu^{2+} resulted in the aggregation and subsequent luminescence quenching of QCs, a control experiment was carried out with ethylenediaminetetraacetate (EDTA). EDTA can chelate or complex with metal ions in a 1:1 ratio and Cu^{2+} has more affinity towards EDTA than BSA. When EDTA was added to the Au_{QC}@BSA + Cu^{2+} mixture, an EDTA–Cu^{2+} complex was formed resulting in the deaggregation of Au_{QC}@BSA clusters. This resulted in the recurrence of luminescence of the QC. The luminescence was recovered as a function of EDTA concentration (Supporting Information, Figure S8A) and recovery was complete when an equal amount of EDTA (to that of Cu^{2+}) was added to the mixture. The TEM images after the addition showed no spherical aggregates (Supporting Information, Figure S8B). To further confirm the results, the QC was first treated with EDTA and Cu^{2+} ions were added subsequently. In this case no quenching was observed and no aggregates were formed.

The recovery of luminescence on addition of EDTA can be used as a "turn-on" luminescence sensor for other molecules. Moreover, because the QC is highly water soluble, it can be used for the detection of biologically and environmentally important molecules. We used this strategy for the detection of a biologically relevant molecule, reduced glutathione. Glutathione is a tripeptide consisting of the amino acids L-cysteine, L-glutamic acid, and glycine. It is produced in the cells to function as an antioxidant for the neutralization of free radicals and reactive oxygen compounds. Glutathione is a better chelating agent for Cu^{2+} than BSA. It will form a complex with Cu^{2+} ions in 2:1 (glutathione/Cu^{2+}) ratio. An aqueous solution of reduced glutathione was added to the mixture containing QCs ($0.1\,mg\,mL^{-1}$) and Cu^{2+} ions (1 μM). The addition of glutathione resulted in the formation of a complex between Cu^{2+} ions and glutathione. This resulted in the deaggregation of Au_{QC}@BSA clusters with recurrence of luminescence. The luminescence recovered as a function of glutathione concentration and complete recovery took place by the addition of 2 μM equivalent of glutathione (see Figure 7).

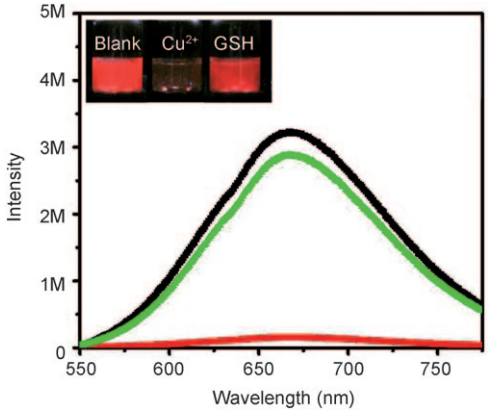

Figure 7. Recovery of the photoluminescence intensity of the Au_{QC}@BSA + Cu^{2+} mixture after the addition of glutathione (GSH; black = cluster, red = cluster + Cu^{2+}, and green = cluster + Cu^{2+} + GSH). Inset: the corresponding photographs.

We also demonstrated the metal-enhanced fluorescence (MEF) of Au_{QC}@BSA in the presence of AgNPs and gold–silver (1:1) alloy nanoparticles (AuAgNPs). The MEF of organic fluorophores[50–54] as well as semiconductor quantum dots[55,56] has been demonstrated. However, there are no studies on the MEF of QCs and this is the first report. When a fluorophore is directly bound to metal nanoparti-

cles, its fluorescence quenches. On the other hand, when they are separated by a distance, the fluorescence enhances.[50] This effect is known as MEF. Metallic nanoparticles can have dramatic effects on the fluorescence of fluorophores, such as increased QYs, decreased molecular excited-state lifetimes, and increased photostability.[50] The fluorescence enhancement is attributable to a combination of processes including enhanced absorption by the molecule, modification of the radiative decay rate of the molecule, and enhanced coupling efficiency of the fluorescence emission to the far field. Recently, fluorescence enhancement of the NIR fluorophore IR800 by Au nanoshells and Au nanorods has been demonstrated.[50] HSA served as a spacer layer between the nanoparticle and the fluorophore. This study shows that proteins can act as a spacer for MEF. We selected three systems for the MEF study: citrate-capped AgNPs, AuNPs, and AuAgNPs. Au_{QC}@BSA (0.5 mg mL^{-1}) was added to the as-synthesized nanoparticles (200 μL mL^{-1}) and the mixture was stirred for 5 h. The BSA shell of the QC acts as the spacer between the QC and the nanoparticles. The optical absorption spectra of the nanoparticles before and after the addition of Au_{QC}@BSA are given in the Supporting Information, Figure S9. There is a slight redshift in the surface plasmon resonance of the nanoparticles after the addition of QCs, which may be due to the change in refractive index of the solution. A plot of the luminescence intensity of Au_{QC}@BSA in the presence and absence of nanoparticles is given in Figure 8 A. Approximately ninefold enhancement of luminescence was observed for the QCs in the presence of AgNPs. There was no enhancement of luminescence for AuNPs and AuAgNPs. However, the nanoparticles exhibit almost no luminescence in the absence of Au_{QC}@BSA. The reason for the nonenhancement of luminescence in the case of AuNPs and AuAgNPs can be attributed to the poor matching of the excitation wavelength and the surface plasmon oscillations of the nanoparticles. The lifetime of the QC before and after treatment with AgNPs was measured to check whether there was any decrease in the excited-state lifetime (see Table 1). The major intrinsic lifetime component of the QC was 0.10 ns (59.6 %) and it was reduced to 0.02 ns (84.6 %) in the presence of AgNPs. There was also a corresponding decrease in the other lifetime components. This enhancement in luminescence and reduction in the excited-state lifetime confirms MEF. As the nature of emission is unclear, we designate it as luminescence and refer to the phenomenon as metal-enhanced luminescence (MEL).

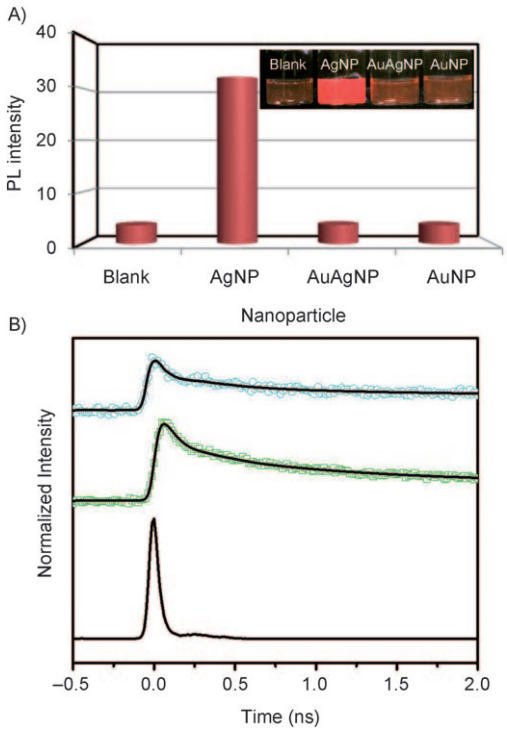

Figure 8. A) MEL of Au_{QC}@BSA in the presence of AgNPs, AuAgNPs, and AuNPs. Inset: photograph of the corresponding aqueous solutions under irradiation by UV light. B) Photoluminescence decay of pure Au_{QC}@BSA (green) and Au_{QC}@BSA in the presence of AgNPs (blue); instrument response function (bottom graph).

Table 1. Lifetime data of pure Au_{QC}@BSA and Au_{QC}@BSA in the presence of AgNPs.

Sample	τ_1 [ns]	%	τ_2 [ns]	%	τ_3 [ns]	%	τ_4 [ns]	%
Blank	0.10	59.6	0.86	21.9	4.5	08.6	174.7	09.9
AgNPs	0.02	84.6	0.30	07.0	3.0	04.0	166.5	04.4

Au_{QC}@BSA is luminescent in the pH window of 2–12 (data not shown) and hence can be used as a staining agent for various imaging applications including cell imaging. The advantage of using QCs for live-cell imaging is twofold, when compared to organic fluorophores and semiconductor quantum dots. Organic fluorophores are prone to photobleaching whereas QCs are comparatively photostable. Semiconductor quantum dots are made up of toxic elements such as Cd and Pb, and they have to be functionalized with biological molecules to decrease cytotoxicity. On the other hand, QCs are made up of the relatively nontoxic element gold and the metallic content is very low (number of core atoms is very low). We used a process called receptor-mediated endocytosis (RME) for the uptake of QCs by cells. RME is a process by which cells internalize molecules (endocytosis) by the inward budding of plasma membrane vesicles containing proteins with receptor sites specific to the molecules being internalized. FA-mediated endocytosis is one such process and has been used for cell uptake and subsequent imaging studies. Certain cancerous cells, such as ovarian, oral, and breast, are rich in FA receptors and they can internalize molecules conjugated with FA. Here we functionalized the QCs with FA following 1-ethyl-3-(3-dimethylaminopropyl)carbodiimide (EDC) coupling of FA and BSA.[57] The FA-functionalized QC was characterized by optical absorption and emission (Supporting Information, Figure S10). Oral carcinoma KB cells have increased folate receptor and were used for uptake studies. Mouse fibroblast L929 cells without any folate receptor were used as negative

control. For folate-targeted imaging, folate receptors were unregulated by maintaining the cells in FA-depleted RPMI medium at 37 °C with 5 % CO_2 for 3 weeks. FA-conjugated QCs were added at a concentration of 1 mg mL^{-1} to both KB and L929 cells. The cells were incubated with the QCs for 24 h. After that the cells were washed with phosphate-buffered saline (PBS) of pH 7.4 to remove any nonspecific attachment of QCs. The cells were fixed and imaged by fluorescence microscopy. The QC luminescence was detected using bandpass excitation and emission filters (480–550 nm excitation, 590 nm emission, and 570 nm dichromatic mirrors). An intense luminescence was observed from the KB cells (see Figure 9). This luminescence was from the QCs internalized by the cell. On the other hand, no significant luminescence was observed for L929 cells, which contain very few FA receptors. These two experiments confirm that the internalization occurred by FA-mediated endocytosis. Cancerous cells contain a large number of folate receptors when compared to normal cells, and therefore FA-conjugated Au_{QC}@BSA can be used for the detection of cancer cells.

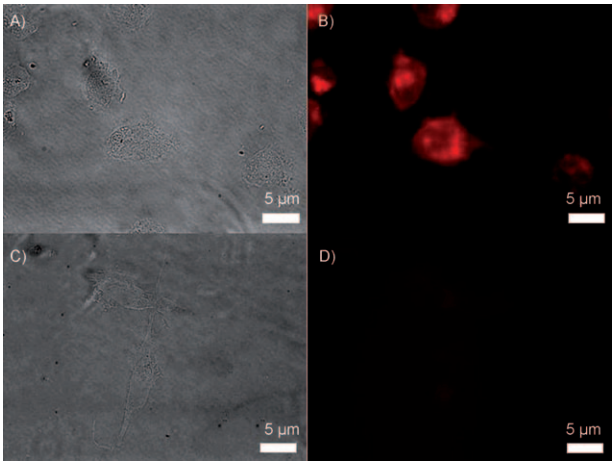

Figure 9. Bright-field (A,C) and the corresponding fluorescence microscopy (B,D) images showing the interaction of FA-conjugated Au_{QC}@BSA with different types of cell lines. Upper panel: images of folate-receptor-positive KB cells with FA-conjugated Au_{QC}@BSA incubated for 24 h; lower panel: images of folate-receptor-negative mouse fibroblast L929 cells with FA-conjugated Au_{QC}@BSA incubated for 24 h.

Conclusion

The synthesis of luminescent QCs of gold with a QY of 4 % is reported. The QCs were synthesized by the core etching of AuNPs by BSA. BSA has long been used as a reducing as well as capping agent for synthesizing nanoparticles. This is the first report of the use of a biomolecule such as BSA as the etching agent for the synthesis of QCs. The synthesized QC is characterized thoroughly and found to have a core of Au_{38}. Luminescence of the QC is exploited as a "turn-off" sensor for the detection of the Cu^{2+} ion and a "turn-on" sensor for glutathione detection. The MEL of this QC in the presence of AgNPs is demonstrated and is found to have a maximum ninefold enhancement. This is also the first report of the observation of MEL from QCs. The QCs are internalized after conjugating with FA by oral carcinoma KB cells by a process called FA-mediated endocytosis. The stability of the clusters in a large pH range, and their continued luminescence, solvent stability, and limited change in secondary structure make them very interesting for diverse applications.

Experimental Section

Materials: Tetrachloroauric acid trihydrate ($HAuCl_4 \cdot 3H_2O$) was purchased from CDH, India. Mercaptosuccinic acid (MSA), sodium borohydride ($NaBH_4$), 1-ethyl-3-(3-dimethylaminopropyl)carbodiimide hydrochloride (EDC), folic acid (FA), and silver nitrate ($AgNO_3$) were purchased from Sigma–Aldrich. BSA was purchased from Fluka. Trisodium citrate was purchased from Sisco Research Laboratories. All chemicals were used without further purification. Triply distilled water was used throughout the experiments. Solvents were of analytical grade.

Synthesis of MSA-capped AuNPs (Au_{NP}@MSA): Au_{NP}@MSA was synthesized according to an earlier report with a slight modification.[42] MSA (20 mM) was added to $HAuCl_4 \cdot 3H_2O$ in methanol (100 mL, 5 mM). The mixture was then cooled to 0 °C in an ice bath for 2 h. An aqueous solution of $NaBH_4$ (25 mL, 0.2 M), cooled at 0 °C, was injected rapidly into this mixture under vigorous stirring. The mixture was allowed to react for another hour. The resulting precipitate was collected and washed repeatedly with methanol/water through centrifugal precipitation and dried to obtain the Au_{NP}@MSA as a dark brown powder.

Synthesis of Au_{QC}@BSA: As-synthesized Au_{NP}@MSA (10 mg) was dissolved in distilled water (5 mL). The pH of the solution was adjusted to 12 by adding NaOH. BSA (100 mg) was added to the solution and the mixture was stirred well for 5 min. The pH of the resulting solution was readjusted to 12 if necessary and the solution was stirred for 6–8 h at 37 °C. The solution was centrifuged at 20000 rpm for 30 min to separate the QCs, which were dialyzed extensively against doubly distilled water for 24 h with a water change every 8 h. The solvent was evaporated by freeze-drying and the product was stored as a powder. No additional products were detected.

Synthesis of AgNPs:[43] A stock solution of $AgNO_3$ in water (200 mL, 0.005 M) was diluted to 1 L and heated until it began to boil. Sodium citrate solution (40 mL, 1 %) was added and heating continued until the color was pale yellow.

Synthesis of AuAgNPs:[44] For the synthesis of alloy nanoparticles, the total concentration of metal ions (including $HAuCl_4$ and $AgNO_3$) was kept at 0.25 mM. In the first step, an appropriate volume of $HAuCl_4$ aqueous solution (30 mM) was added to water (50 mL), and the mixture was heated to its boiling temperature. Aqueous $AgNO_3$ solution (20 mM) of appropriate volume was added to the hot solution. Sodium citrate solution (2.5 mL, 1 %) was added to the solution heated at reflux, and the solution continued to be heated for another 30 min. The final solution was then left to cool to room temperature.

Conjugation of FA with Au_{QC}@BSA:[57] QCs were conjugated with FA with the zero-length cross-linker EDC. FA was activated to become amine-reactive by linking with EDC. EDC (8.3 mg) was added to FA (3.3 mg) in PBS (500 μL; 136.9 mM NaCl, 2.68 mM KCl, 8.1 mM Na_2HPO_4, 1.47 mM KH_2PO_4, pH 7.4) and the mixture was incubated for 15 min in the dark at room temperature with probe sonication. The activated FA was added to QCs (50 mg) dissolved in PBS (5 mL). The solution was stirred overnight at room temperature; then the pH of the reaction mixture was adjusted to 9 and the solution was promptly passed through a desalting column (Zeba Desalt Spin Columns provided by Thermo Scientific, India). Alkalization of the reaction mixture was necessary for the

complete separation of free folate from the conjugate. Successful conjugation of FA to QC was confirmed by FTIR and UV/Vis absorption spectroscopy.

Instrumentation: UV/Vis spectra were measured in the range of 200–1100 nm with a Perkin–Elmer Lambda 25 instrument. The FTIR spectra were measured with a Perkin–Elmer Spectrum One instrument. KBr crystals were used as the matrix for sample preparation. Fluorescence measurements were carried out on a Jobin Yvon NanoLog instrument. The bandpass for excitation and emission was set as 5 nm. XPS measurements were conducted with an Omicron ESCA Probe spectrometer with polychromatic $Mg_{K\alpha}$ X-rays ($h\nu = 1253.6$ eV). The samples were spotted as drop-cast films on a sample stub. A constant analyzer energy of 20 eV was used for the measurements. MALDI-MS studies were conducted with a Voyager DE PRO Biospectrometry Workstation (Applied Biosystems). A pulsed nitrogen laser operating at 337 nm was used for the studies. Mass spectra were collected in positive-ion mode and were averaged for 50 shots. ESIMS data were collected with an Applied Biosystems QTrap3200 MS/MS instrument. The samples in water/methanol (1:1) were electrosprayed at 5 kV; TFA (10 μL, 1 %) was also added. The spectra were averaged for 100 scans. Fluorescence transients were measured and fitted by using a commercially available spectrophotometer (LifeSpec-ps) from Edinburgh Instruments, UK (80 ps instrument response function). The QCs were excited at 409 nm and the emission decays were collected at 660 nm. EDX analysis was carried out with an FEI QUANTA-200 SEM instrument and the samples were prepared on conducting ITO glass plates. A Leica TCS SP2-AOBS confocal microscope was used for imaging the cells by exciting them with a 514 nm laser. Emission between 600 and 800 nm was collected. The CD studies were carried out in a JASCO 815 spectrometer with an attachment for the temperature-dependent measurements (Peltier). CD studies were performed in a 1.0 cm path length cell. The secondary structural data of the CD spectra were analyzed with CDNN software.[58] Fluorescence images of the cells were obtained with an Olympus BX-51 fluorescence microscope equipped with a color CCD camera (Model DP71) with 60× oil immersion objectives.

Acknowledgements

We thank the Department of Science and Technology, Government of India for constantly supporting our research program on nanomaterials.

[1] P. A. Bartlett, B. Bauer, S. Singer, *J. Am. Chem. Soc.* **1978**, *100*, 5085–5089.
[2] G. Schmid, R. Boese, B. Pfeil, F. Andermann, S. Meyer, G. H. M. Calis, J. W. A. Van der Velden, *Chem. Ber.* **1981**, *114*, 3634–3642.
[3] J. Zheng, J. T. Petty, R. M. Dickson, *J. Am. Chem. Soc.* **2003**, *125*, 7780–7781.
[4] J. Zheng, C. W. Zhang, R. M. Dickson, *Phys. Rev. Lett.* **2004**, *93*, 077402/1–4.
[5] J. Zheng, P. R. Nicovich, R. M. Dickson, *Annu. Rev. Phys. Chem.* **2007**, *58*, 409–431.
[6] C.-A. J. Lin, T.-Y. Yang, C.-H. Lee, S. H. Huang, R. A. Sperling, M. Zanella, J. K. Li, J.-L. Shen, H.-H. Wang, H.-I. Yeh, W. J. Parak, W. H. Chang, *ACS Nano* **2009**, *3*, 395–401.
[7] R. Archana, S. Sonali, M. Deepthy, R. Prasanth, M. A. Habeeb Muhammed, T. Pradeep, N. Shantikumar, K. Manzoor, *Nanotechnology* **2010**, *21*, 055103(1–12).
[8] M. A. Habeeb Muhammed, P. K. Verma, S. K. Pal, R. C. Arun Kumar, S. Paul, R. V. Omkumar, T. Pradeep, *Chem. Eur. J.* **2009**, *15*, 10110–10120.
[9] G. Ramakrishna, O Varnavski, J. Kim, D. Lee, T. Goodson, *J. Am. Chem. Soc.* **2008**, *130*, 5032–5033.
[10] M. A. Habeeb Muhammed, A. K. Shaw, S. K. Pal, T. Pradeep, *J. Phys. Chem. C* **2008**, *112*, 14324–14330.
[11] J. I. Gonzalez, T.-H. Lee, M. D. Barnes, Y. Antoku, R. M. Dickson, *Phys. Rev. Lett.* **2004**, *93*, 147402/1–4.
[12] Y. Negishi, K. Nobusada, T. Tsukuda, *J. Am. Chem. Soc.* **2005**, *127*, 5261–5270.
[13] Y. Shichibu, Y. Negishi, T. Tsukuda, T. Teranishi, *J. Am. Chem. Soc.* **2005**, *127*, 13464–13465.
[14] Y. Shichibu, Y. Negishi, H. Tsunoyama, M. Kanehara, T. Teranishi, T. Tsukuda, *Small* **2007**, *3*, 835–839.
[15] Y. Negishi, Y. Takasugi, S. Sato, H. Yao, K. Kimura, T. Tsukuda, *J. Am. Chem. Soc.* **2004**, *126*, 6518–6519.
[16] M. A. Habeeb Muhammed, T. Pradeep, *Chem. Phys. Lett.* **2007**, *449*, 186–190.
[17] E. S. Shibu, M. A. Habeeb Muhammed, T. Tsukuda, T. Pradeep, *J. Phys. Chem. C* **2008**, *112*, 12168–12176.
[18] E. S. Shibu, B. Radha, P. K. Verma, P. Bhyrappa, G. U. Kulkarni, S. K. Pal, T. Pradeep, *ACS Appl. Mater. Interfaces* **2009**, *1*, 2199–2210.
[19] M. A. Habeeb Muhammed, S. Ramesh, S. S. Sinha, S. K. Pal, T. Pradeep, *Nano Res.* **2008**, *1*, 333–340.
[20] J. Xie, Y. Zheng, J. Y. Ying, *J. Am. Chem. Soc.* **2009**, *131*, 888–889.
[21] T. G. Schaaff, M. N. Shafigullin, J. T. Khoury, I. Vezmar, R. L. Whetten, *J. Phys. Chem. B* **1997**, *101*, 7885–7891.
[22] T. G. Schaaff, G. Knight, M. N. Shafigullin, R. F. Borkman, R. L. Whetten, *J. Phys. Chem. B* **1998**, *102*, 10643–10646.
[23] S. Link, A. Beeby, S. F. Gerald, M. A. El-Sayed, T. G. Schaaff, R. L. Whetten, *J. Phys. Chem. B* **2002**, *106*, 3410–3415.
[24] R. C. Price, R. L. Whetten, *J. Am. Chem. Soc.* **2005**, *127*, 13750–13751.
[25] Z. Wu, J. Suhan, R. Jin, *J. Mater. Chem.* **2009**, *19*, 622–626.
[26] M. Zhu, E. Lanni, N. Garg, M. E. Bier, R. Jin, *J. Am. Chem. Soc.* **2008**, *130*, 1138–1139.
[27] M. Zhu, H. Qian, R. Jin, *J. Am. Chem. Soc.* **2009**, *131*, 7220–7221.
[28] H. Qian, M. Zhu, U. N. Andersen, R. Jin, *J. Phys. Chem. A* **2009**, *113*, 4281–4284.
[29] H. Qian, M. Zhu, E. Lanni, Y. Zhu, M. E. Bier, R. Jin, *J. Phys. Chem. C* **2009**, *113*, 17599–17603.
[30] M. Zhu, C. M. Aikens, F. J. Hollander, G. C. Schatz, R. Jin, *J. Am. Chem. Soc.* **2008**, *130*, 5883–5885.
[31] G. Wang, R. Guo, G. Kalyuzhny, J.-P. Choi, R. W. Murray, *J. Phys. Chem. B* **2006**, *110*, 20282–20289.
[32] M. W. Heaven, A. Dass, P. S. White, K. M. Holt, R. W. Murray, *J. Am. Chem. Soc.* **2008**, *130*, 3754–3755.
[33] A. Dass, A. Stevenson, G. R. Dubay, J. B. Tracy, R. W. Murray, *J. Am. Chem. Soc.* **2008**, *130*, 5940–5946.
[34] H. Duan, S. Nie, *J. Am. Chem. Soc.* **2007**, *129*, 2412–2413.
[35] J. T. Petty, J. Zheng, N. V. Hud, R. M. Dickson, *J. Am. Chem. Soc.* **2004**, *126*, 5207–5212.
[36] S. H. Brewer, W. R. Glomm, M. C. Johnson, M. K. Knag, S. Franzen, *Langmuir* **2005**, *21*, 9303–9307.
[37] A. V. Singh, B. M. Bandgar, M. Kasture, B. L. V. Prasad, M. Sastry, *J. Mater. Chem.* **2005**, *15*, 5115–5121.
[38] J. A. Dahl, B. L. S. Maddux, J. E. Hutchison, *Chem. Rev.* **2007**, *107*, 2228–2269.
[39] D. Mandal, M. E. Bolander, D. Mukhopadhayay, G. Sarkar, P. Mukherjee, *Appl. Microbiol. Biotechnol.* **2006**, *69*, 485–492.
[40] P. Murawalaa, S. M. Phadnisb, R. R. Bhondeb, B. L. V. Prasad, *Colloids Surf. B* **2009**, *73*, 224–228.
[41] N. El Kadi, N. Taulier, J. Y. Le Huérou, M. Gindre, W. Urbach, I. Nwigwe, P. C. Kahn, M. Waks, *Biophys. J.* **2006**, *91*, 3397–3404.
[42] S. Sato, S. Wang, K. Kimura, *J. Phys. Chem. C* **2007**, *111*, 13367–13371.
[43] P. V. Kamat, M. Flumiani, G. V. Hartland, *J. Phys. Chem. B* **1998**, *102*, 3123–3128.
[44] Y. Sun, Y. Xia, *Analyst* **2003**, *128*, 686–691.
[45] O. Varnavski, G. Ramakrishna, J. Kim, D. Lee, T. Goodson, *J. Am. Chem. Soc.* **2010**, *132*, 16–17.
[46] P. Ramasamy, S. Guha, E. S. Shibu, T. S. Sreeprasad, S. Bag, A. Banerjee, T. Pradeep, *J. Mater. Chem.* **2009**, *19*, 8456–8462.
[47] K. Fua, K. Griebenowb, L. Hsiehc, A. M. Klibanovd, R. Langera, *J. Controlled Release* **1999**, *58*, 357–366.

[48] T. Maruyamaa, S. Katoh, M. Nakajima, H. Nabetani, T. P. Abbott, A. Shono, K. Satoh, *J. Membr. Sci.* **2001**, *192*, 201–207.
[49] R. A. Løvstad, *BioMetals* **2004**, *17*, 111–113.
[50] R. Bardhan, N. K. Grady, J. R. Cole, A. Joshi, N. J. Halas, *ACS Nano* **2009**, *3*, 744–752.
[51] C. D. Geddes, I. Gryczynski, J. Malicka, Z. Gryczynski, J. R. Lakowicz, *Comb. Chem. High Throughput Screening* **2003**, *6*, 109–117.
[52] K. Aslan, M. Wu, J. R. Lakowicz, C. D. Geddes, *J. Am. Chem. Soc.* **2007**, *129*, 1524–1525.
[53] R. Badugu, J. R. Lakowicz, C. D. Geddes, *J. Am. Chem. Soc.* **2005**, *127*, 3635–3641.
[54] J. Zhang, Y. Fu, M. H. Chowdhury, J. R. Lakowicz, *Nano Lett.* **2007**, *7*, 2101–2107.
[55] K. Ray, R. Badugu, J. R. Lakowicz, *J. Am. Chem. Soc.* **2006**, *128*, 8998–8999.
[56] Y-H. Chan, J. Chen, S. E. Wark, S. L. Skiles, D. H. Son, J. D. Batteas, *ACS Nano* **2009**, *3*, 1735–1744.
[57] R. J. Lee, S. Wang, P. S. Low, *Biochim. Biophys. Acta Mol. Cell Res.* **1996**, *1312*, 237–242.
[58] G. Böhm, R. Muhr, R. Jaenicke, *Protein Eng.* **1992**, *5*, 191–195.
[59] J. Sommer-Knudsen, A. Bacic, *Mol. Biotechnol.* **1997**, *8*, 215–218.

Received: April 3, 2010
Published online: July 7, 2010

